ADVANCED HEALTHCARE MATERIALS
www.advhealthmat.de

Core–Shell Composite Hydrogels for Controlled Nanocrystal Formation and Release of Hydrophobic Active Pharmaceutical Ingredients

*Abu Zayed Md Badruddoza, P. Douglas Godfrin, Allan S. Myerson, Bernhardt L. Trout, and Patrick S. Doyle**

Although roughly 40% of pharmaceuticals being developed are poorly water soluble, this class of drugs lacks a formulation strategy capable of producing high loads, fast dissolution kinetics, and low energy input. In this work, a novel bottom-up approach is developed for producing and formulating nanocrystals of poorly water-soluble active pharmaceutical ingredients (APIs) using core–shell composite hydrogel beads. Organic phase nanoemulsion droplets stabilized by polyvinyl alcohol (PVA) and containing a model hydrophobic API (fenofibrate) are embedded in the alginate hydrogel matrix and subsequently act as crystallization reactors. Controlled evaporation of this composite material produces core–shell structured alginate-PVA hydrogels with drug nanocrystals (500–650 nm) embedded within the core. Adjustable loading of API nanocrystals up to 83% by weight is achieved with dissolution (of 80% of the drug) occurring in as little as 30 min. A quantitative model is also developed and experimentally validated that the drug release patterns of the fenofibrate nanocrystals can be modulated by controlling the thickness of the PVA shell and drug loading. Thus, these composite materials offer a "designer" drug delivery system. Overall, our approach enables a novel means of simultaneous controlled crystallization and formulation of hydrophobic drugs that circumvents energy intensive top–down processes in traditional manufacturing.

1. Introduction

Advances in nanotechnology have facilitated the engineering of functional structures at the nanoscale. A prominent example is the synthesis of nanoparticles and organic nanocrystals that have a large potential impact for many applications, such as pharmaceuticals, foods, and cosmetics.[1] Materials prepared on the nanoscale have markedly improved physicochemical properties compared to their bulk counterparts. In particular, active pharmaceutical ingredients (APIs) prepared in the nanometer size range (<1000 nm) offer increases in solubility and dissolution rates.[2] This may help overcome the typical issues with hydrophobic APIs, such as solubility-limited oral bioavailability and erratic absorption, which limits the development of many highly potent pharmaceutics. Approximately 40% of newly developed drugs are extremely hydrophobic, and this number is gradually increasing.[3] Developing new technology for the synthesis of nanocrystalline drugs can facilitate the formulation of these poorly soluble yet valuable APIs.

Over the past few years, major research efforts have been focused on the development of API nanocrystals and nanoformulations. The conventional methods for the production of API nanocrystals are jet milling using pearl/ball mills (e.g., NanoCrystals),[4] high-pressure homogenization,[5] and antisolvent precipitation.[6] However, due to stability and/or patient compliance reasons, these formulations need to be transformed into more preferred, conventional solid dosage forms (e.g., tablets, capsules, pellets).[7,8] Typically, the liquid to solid (crystalline or amorphous) transformation is achieved by spray drying, lyophilization, pelletization, and granulation.[8] The drawbacks of preparing nanocrystalline APIs by these techniques are numerous, the most prominent of which are high production costs, a low drug to carrier ratio, agglomeration of drug nanoparticles, and low polymorph purity.[9,10] Therefore, the preferential fabrication of nanocrystalline APIs for oral delivery would directly produce solid dosage formulations. The ideal process should accommodate the encapsulation of hydrophobic, hydrophilic or both types of drugs with high loading capacity and stability, while also delivering an accurate dosage in a time-controlled manner. It remains a major challenge to design a process which meets the aforementioned nanoparticle formulation requirements and is versatile enough to allow for continued development and scale-up.

In recent years, biocompatible polymeric hydrogels have been widely exploited as promising encapsulating and delivery matrix materials for APIs.[11,12] However, due to the hydrophilicity of hydrogels, their ability to encapsulate and release water insoluble pharmaceuticals still remains a challenge. Different strategies are being developed in order to exploit the advantages

Dr. A. Z. M. Badruddoza, Dr. P. D. Godfrin,
Prof. A. S. Myerson, Prof. B. L. Trout, Prof. P. S. Doyle
Department of Chemical Engineering
Massachusetts Institute of Technology
77 Massachusetts Avenue, Cambridge, MA 02139, USA
E-mail: pdoyle@mit.edu

DOI: 10.1002/adhm.201600266

of hydrogels and implement them as formulation vehicles for hydrophobic drugs. One strategy is to incorporate hydrophobic domains or compartments into the hydrogel matrix using either nanoparticles,[13] emulsions,[14] and microemulsions.[15] The encapsulation of nanoemulsions (kinetically stabilized suspensions of nanosized oil droplets) within a hydrogel matrix has been demonstrated as an effective method for controlled drug release.[16] The small size and monodisperse size population of nanoemulsions relative to typical macroemulsions produces greater kinetic stability of the droplets, which improves shelf life and ease of use when integrating into other materials. Solvent in the droplets can be evaporated to induce crystallization. The small size of the nanoemulsions translates into a small crystal sizes that enhances release kinetics and bioavailability. In addition, the ability to produce nanoemulsions at high volume fractions allows for precise control of loading within the hydrogel, while the ability to tune the hydrogel network allows for a controlled barrier to release. Although such hydrogel composites are promising, current approaches compromise API loading for faster release rates.[17] Further, some systems have no control over one or more of these important aspects, including crystal size and drug release rate.[18,19]

Core–shell polymeric particles have shown great potential in many applications, but particularly pharmaceutical drug delivery, owing to their hybrid chemical composition and unique layered geometry that produce advanced encapsulation properties.[20–26] By utilizing materials that offer increased drug solubility in the core phase, higher drug loading with improved drug stability may be realized while also protecting incorporated drugs from premature degradation, undesired reactions or evaporation. In particular, the development of biodegradable polymeric core–shell hydrogels to specifically protect sensitive materials (e.g., drugs, therapeutics, cells) has been a major focus of pharmaceutical and materials research.[21,27] The integration of biodegradable materials permits greater flexibility to optimize the degradation rate of the core–shell particle, including modulated release kinetics of encapsulated APIs. Advanced drug release schedules such as delayed or pulsatile release, without an initial burst, may be possible by selectively varying the shell material or thickness. Therefore, introduction of an additional shell layer on polymeric microspheres or microgels can significantly improve their versatility as well as functionality as delivery vehicles. Guo et al. have shown that the shell delays the degradation of the hydrogel core and release of the embedded organic substance.[22] In this instance they used FITC–dextran loaded core–shell capsules comprising biodegradable modified poly(ethylene glycol) and alginate.[22] Wu et al. prepared uniform PLGA-alginate (core–shell, respectively) particles by the capillary microfluidic method and showed that the drug release kinetics could be modulated either by the core size or shell thickness.[23]

In this study, we report a novel approach for generating nanocrystals of a model, poorly water-soluble API, fenofibrate (FEN), embedded in a polymeric matrix with controlled crystal size and drug loading capacity. We further demonstrate control over the release kinetics by utilizing the unique microstructure of biodegradable core–shell hydrogels. Fenofibrate is a Biopharmaceutics Classification System (BCS) class II drug, which is very lipophilic and practically insoluble in water.[28] We use a facile method to fabricate core–shell composite hydrogels composed of an alginate core with polyvinyl alcohol (PVA) shell. Hydrophobic (organic phase) nanoemulsion droplets containing soluble fenofibrate are embedded in the hydrogel polymer matrix using PVA as an emulsifying agent, and act as crystallization reactors. By controlled evaporation of this composite material, core–shell structured hydrogel with FEN nanocrystals of controlled size (500–650 nm) embedded within the core are produced. This process allows the size and loading of API nanocrystals (up to 83% by weight) and the thickness of PVA shell on composite hydrogels to be tuned, which subsequently modulates the drug release behavior. Thus, our composite hydrogel beads offer an oral delivery system built for controlled crystallization and modulated release of water-insoluble drugs.

2. Results and Discussion

A schematic diagram of the formation of a composite hydrogel with a core–shell microstructure is shown in **Figure 1**. Generating the core–shell hydrogel material is a multistep process that begins with preparing the oil in water nanoemulsions by emulsifying the hydrophobic organic phase (anisole) saturated with FEN in an aqueous solution containing the biocompatible polymer alginate (ALG) and PVA. The PVA is used for stabilizing the nanoemulsion droplets. PVA is an FDA-approved GRAS (generally recognized as safe) material and has been widely used as an emulsifier, binder, and film coating agent in the food and pharmaceuticals industries. Anisole is chosen as the dispersed phase due to its approval for pharmaceutical manufacturing and the high saturation concentration (C_{satFEN}) of fenofibrate in this solvent (≈400 mg mL^{-1}).[17] Nanoemulsions are produced by ultrasonication,[29] which is a robust process for preparing droplets across a range of sizes. ALG beads are produced by dripping the uncrosslinked nanoemulsion dispersion into a 6%, w/v $CaCl_2$ bath in drop-wise fashion. The final bead size depends on the composition of the nanoemulsion solutions and the diameter of the needle. Ionic crosslinking of ALG creates a crosslinked polymer network trapping the nanoemulsion droplets containing the API. Crystallization of FEN is induced by controlled evaporation of both the dispersed organic phase and the aqueous phase at 60 °C. During this drying process, we find that the PVA molecules migrate from the aqueous–organic interface to the external surface of the beads, which results in the formation of hydrogel beads with a core–shell microstructure. This approach enables the shell thickness to be engineered either by varying the volume fraction of the dispersed phase at constant PVA concentration or by changing the particle size at constant volume fraction. The ability to tune shell thickness offers modulated control of the dissolution behavior of the embedded API, which will be discussed in more detail later.

The size, morphology, and microstructure of the core–shell composite hydrogels are characterized by high-resolution scanning electron microscopy (HR-SEM). **Figure 2** shows SEM images of core–shell composite hydrogels (both with and without API, as a control) representing a typical API nanocrystal formulated microparticle. The composite hydrogel

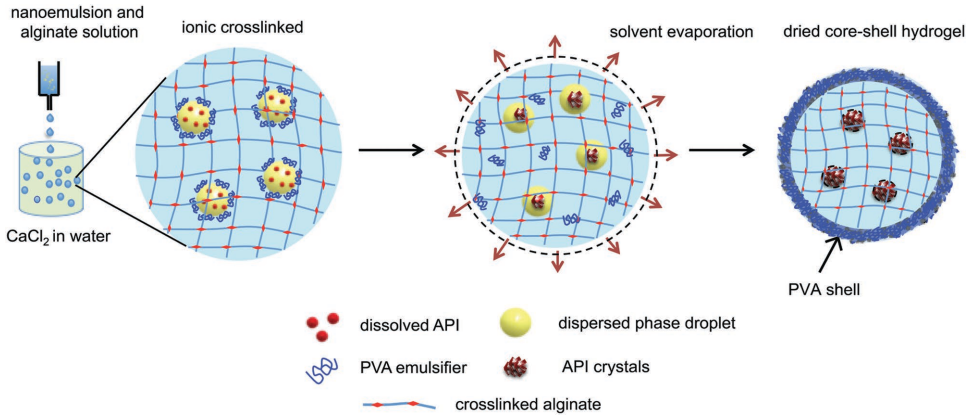

Figure 1. Illustration of the bottom-up approach used in this work to form core–shell composite hydrogel beads. Nanoemulsion droplets stabilized by polyvinyl alcohol (PVA) and carrying a hydrophobic API are dispersed in aqueous solvent containing alginate. The uncrosslinked alginate solution containing nanoemulsions are then dripped through a nozzle into a 6% w/v $CaCl_2$ bath in a drop-wise fashion. Upon crosslinking, the nanoemulsion droplets are entrapped inside the polymer matrix. Crystallization is induced by controlled evaporation of both liquid phases (water and anisole) from the polymer matrix. Once dried, core–shell composite hydrogels are formed containing API nanocrystals embedded in the porous confinement environment of the alginate core.

has a core–shell structure obtained at certain experimental conditions (ϕ = 20% dispersed phase with $C_{FEN} = C_{satFEN}$ emulsified in 2% w/v ALG containing 1% w/v PVA in Figure 2a). Figure 2c also shows FEN nanoparticles confined by pores within the ALG core with some vacant cavities. The presence of the FEN nanocrystals embedded inside the core was further confirmed by Raman spectroscopy (see Figure S1 in the Supporting Information). The control sample which lacks API (Figure 2d,e) shows only vacant pores (1 to 2 µm) with no nanocrystals inside, indicating that the porous alginate matrix facilitates confined crystallization. This control experiment also confirms that the API is not necessary for the shell formation. However, the shell formed in the presence of FEN (Figure 2b) is less conformal than without API (Figure 2e), suggesting that FEN may end up in the shell after drying. Further, producing particles from a mixture of only ALG and PVA does not yield a shell (Figure 2f). The reduced porosity of this control (inset of Figure 2f) is believed to result from the significant excess of PVA in the continuous phase. This result suggests that only the PVA located at the nanoemulsion interface within the crosslinked polymer matrix leads to shell formation after the solvent and water are evaporated. Interestingly, while the dispersed phase is more viscous when saturated with API, which should lead to larger nanoemulsions,[29] formulations with FEN have smaller diameter nanoemulsions (see Table S1 in the Supporting Information) and subsequently smaller pore sizes (compare insets of Figure 2c,e). This suggests that FEN may act as a co-surfactant to stabilize a larger oil–water surface area,

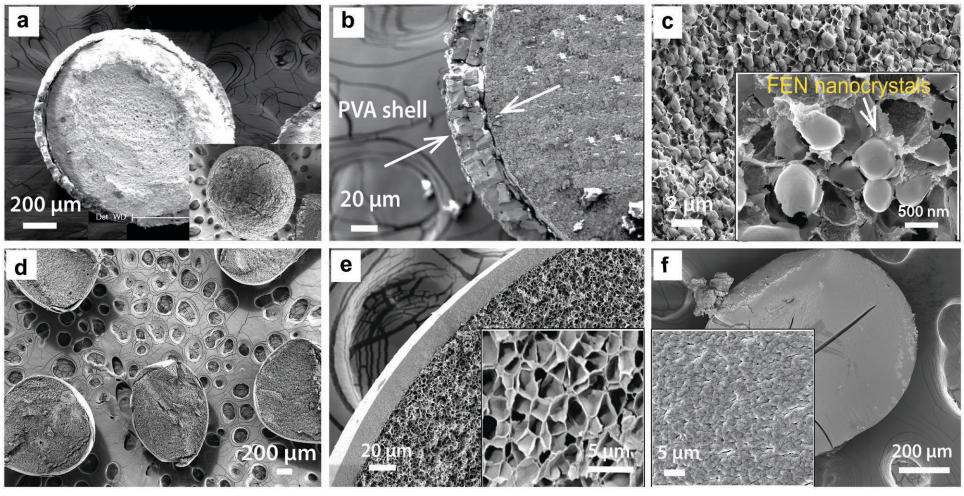

Figure 2. a–c) SEM images of composite core-shell hydrogels embedded with FEN nanocrystals (ϕ = 20% dispersed phase with $C_{FEN} = C_{satFEN}$ emulsified in 2% w/v ALG containing 1% w/v PVA); a) SEM image showing the core–shell structure, b) SEM image displaying the thickness of the composite hydrogel shell constructed with PVA, and c) Cross-sectional view showing the FEN nanocrystals inside microporous polymer matrix. d,e) SEM images of core–shell hydrogels obtained from a control experiment without FEN (ϕ = 20% dispersed phase with C_{FEN} = 0 emulsified in 2% w/v ALG containing 1% w/v PVA). f) SEM image of an ALG hydrogel without oil phase showing no PVA shell (inset shows cross-sectional view) (2% w/v ALG containing 1% w/v PVA).

which is also consistent with the hypothesized integration of FEN into the PVA shell, when present.

To investigate the crystallinity of the API nanocrystals embedded in the dried core–shell hydrogels, we examine the samples by powder X-ray diffraction (PXRD) and differential scanning calorimetry (DSC) (Figure S2 and Figure S3 in the Supporting Information). In Figure S2 (Supporting Information), XRD peaks produced by a typical dried core–shell hydrogel formulation (ϕ = 30% dispersed phase with C_{FEN} = C_{satFEN} emulsified in 2% w/v ALG containing 1% w/v PVA emulsifier) match the peaks of the FEN standard. DSC measurements also exhibit a well-defined endotherm at approximately 81 °C corresponding to the melting point of fenofibrate. Both techniques thus demonstrate that encapsulated FEN nanoparticles are in the crystalline state within the final core–shell structure.

Controlling crystal size is of great importance in pharmaceutical manufacturing as it directly influences the pharmaceutical product performance characteristics such as dissolution rate and bioavailability. In **Figure 3**, we plot both mean nanoemulsion droplet size (< d_d >) measured by dynamic light scattering and mean crystal size (< d_c >) measured by SEM as a function of volume fraction (ϕ) of the dispersed phase. It should be noted that the volume fraction used here to prepare the emulsion laden hydrogels is limited to a maximum of 40%. Above this level, samples form a very foamy and viscous nanoemulsion solution that is difficult to handle. Figure 3 shows that the average droplet size slightly increases from 460 to 630 nm with the increase of volume fraction from 10% to 40%, respectively. This variation of nanoemulsion droplet size corresponds with the shift in the emulsifier (PVA) to dispersed phase ratio. The obtained mean crystal size ranging from 500 to 640 nm (standard deviation of roughly 100 nm each, see the Supporting Information for more details) is nearly identical to the corresponding droplet size, indicating that the size of nanoemulsion droplets dictates the mean crystal size within the dried hydrogel matrix. This approach thus enables precise control

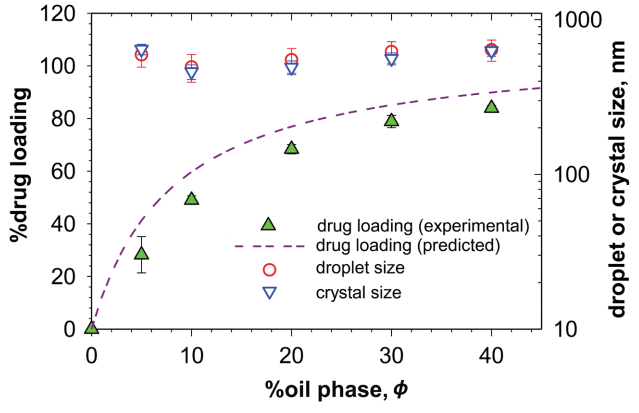

Figure 3. Control of the crystal size and drug loading is shown by manipulating the droplet size at different volume fractions of dispersed phase (ϕ). (continuous phase: 2% w/v ALG aqueous solution with 1% w/v PVA; dispersed phase: anisole with C_{FEN} =C_{satFEN}). Right axis: The mean crystal size (< d_c >) and the mean droplet size (< d_d >) plotted as a function of ϕ. Left axis: Both experimental (symbols) and the theoretical estimate based on Equation (1) (dashed line) of drug loading percent on dry basis are plotted relative to ϕ.

over crystal size and morphology utilizing the elastic nature of the hydrogel matrix and nanoconfinement.[17] Such control is impossible to achieve in traditional evaporation-induced crystallization processes. Further, this is mechanistically different than other approaches that use emulsions to influence crystallization and formulation. There have been recent attempts, using similar methods based on microfluidics and evaporative crystallization, to create microparticles with nanocrystalline hydrophobic drugs embedded in non-hydrogel-based matrices.[30,31] For example, Leon et al. developed an approach to compartmentalize nanocrystalline API within an amorphous polymer matrix by utilizing microfluidic emulsion droplets containing API-polymeric excipient mixtures with subsequent phase separation within the droplets.[30]

Easy manipulation of drug loading is also a powerful feature in pharmaceutical manufacturing since it directly correlates with the dosage of a final formulation. Figure 3 also shows the percentage drug loading at different volume fractions of dispersed phase at the FEN saturation concentration. The amount of FEN embedded in composite hydrogels (% loading on dry basis) can be controlled by tuning the volume fraction of the dispersed phase. To validate our experimental results, we estimated the predicted drug loading capacity based on the saturation concentration of fenofibrate and the formulation concentrations of PVA and alginate according to

$$\%\ \text{drug loading} = (100\%)\frac{C_{FEN}V\phi}{(C_{ALG}+C_{PVA})V(1-\phi)+C_{FEN}V\phi} \quad (1)$$

where $C_{FEN}V\phi$ is the mass of embedded FEN in a hydrogel bead with volume V, C_{ALG}, and C_{PVA} are the concentrations of alginate and PVA, respectively, and $V(1-\phi)$ represents the volume of the continuous phase in a bead. The measured drug loadings are found to be slightly lower than the expected values, which may be due to the loss of some nanoemulsion droplets from hydrogel beads during the crosslinking and washing steps. However, adjustable and high loadings up to 83% can be achieved with relatively narrow distributions (<5%). This is the first demonstration, to the best of our knowledge, to produce nanocrystals of a poorly soluble API with such a high loading using composite hydrogels. In a previous study, Eral et al. were also able to achieve a high loading of 85% FEN using a composite hydrogel matrix.[17] However, this high loading was only with a comparatively large crystal size (>1.1 μm), which produced slow dissolution behavior. Eral et al. also demonstrated a method to prepare nanocrystals of FEN with an average size of 330 nm, but with only 16% of drug loading. Similarly, porous silica materials have also been used for crystallization and formulation of FEN APIs in order to enhance their dissolution and oral bioavailability.[32–35] However, low drug loading and poor crystallinity are major concerns using this formulation technique. For example, Dwyer et al. recently prepared nanocrystals of fenofibrate (30 to 300 nm) by confined crystallization using porous glass materials, but was limited to low drug loading (<30%).[32]

To demonstrate the ability to design specific core–shell structures with this composite system, we develop a scaling law for the outer PVA shell thickness as a function of the formulation parameters. Experimentally, we observed that the shell thickness can be tuned by (1) varying the overall hydrogel

particle size at constant nanoemulsion volume fraction or (2) varying the dispersed phase volume fraction at constant PVA concentration in the continuous phase. Following method (1), core–shell hydrogel particles ranging from 430 to 2100 µm are prepared at constant nanoemulsion volume fraction (ϕ = 30%) using different needle gauges while encapsulated nanocrystals of the API maintain the same size (≈ 620 nm). By method (2), the emulsifier/oil ratio is not maintained constant in all experiments, resulting in a variation of droplet sizes. Furthermore, formulations with a higher volume fraction of the dispersed phase yield hydrogel particles of increased size. Hence, using method (2) each preparation (data point in **Figure 4**) will have a different nanoemulsion volume fraction, nanoemulsion droplet size, and alginate particle size.

Assuming only PVA from the liquid–liquid interfaces in the nanoemulsion migrate to the bead surface (suggested by our SEM control study), the thickness of the shell is expected to scale as:

$$w = A\left(\frac{\phi D_p}{D_d}\right) \quad (2)$$

where, w is thickness of PVA layer, D_p is the diameter of the core–shell particle, D_d is the diameter of emulsion droplets, and ϕ is the volume fraction of dispersed phase. The pre-factor, A, in Equation (2) has dimensions of length and is related to the adsorption cross-section, molecular weight and amorphous density of PVA (see the Supporting Information for more details). Figure 4 shows that the data for PVA shell thickness collapse onto a master curve and is linearly proportional to the dimensionless group $\left[\left(\frac{\phi D_p}{D_d}\right)\right]$. The best fit to the experimental data produced a slope of 0.047 µm, which (combined with other known parameters) yields a value of 8.63 nm^2 for the adsorption cross-section of PVA. This result is reasonable for PVA, which has a radius of gyration of ≈7 nm,[36] suggesting relatively close packing on the oil–water interface yet not quite a brush orientation. As shown in Figure 4, the thickness of the PVA shell can be increased up to ≈60 µm through either of the above experimental approaches by appropriately changing any of the three parameters involved. Though our work is limited to using 1% w/v PVA in the continuous phase, previous studies also indicate that the shell thickness can be altered by varying the concentration and molecular weight of the polymer selected for the shell materials.[37–39] This scaling study shows the versatility of our core–shell composite hydrogels as drug delivery vehicles.

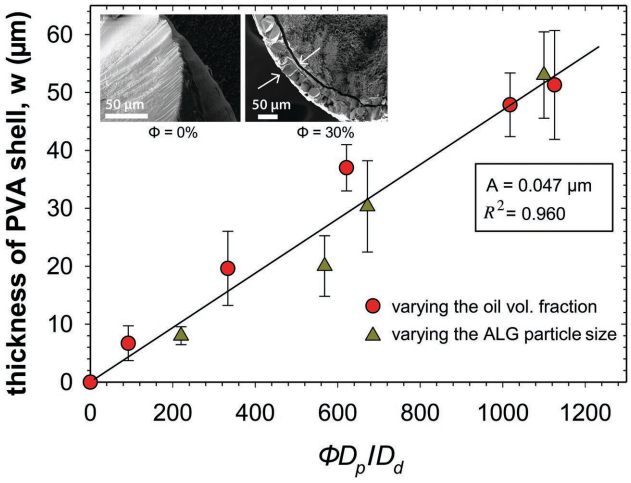

Figure 4. A scaling relationship is shown between the PVA shell thickness on composite core–shell hydrogel beads and formulation parameters. The thickness of the PVA layer can be tuned by varying either the ALG particle size (triangles) or the volume fraction of dispersed phase (circles). The shell thickness is a linear function of the dimensionless group $\left[\phi\left(\frac{D_p}{D_d}\right)\right]$ that includes the volume fraction of dispersed phase (ϕ), alginate particle size (D_p) and emulsion size (D_d). The slope and R^2 values of the best fit to the data using Equation (2) (solid line) are shown in the box.

Simultaneously exploiting porous confinement in the core of our composite particles to control FEN crystal size and the tunable polymeric shell thickness, we can regulate the release/dissolution profile of embedded API. The in vitro dissolution profiles of FEN from the composite core–shell hydrogels prepared by method (1) at a volume fraction of ϕ = 30% are plotted in **Figure 5**. The figure demonstrates that drug is released slower from larger core–shell particles. The dissolution profiles of the larger particles also highlight the presence of two phases, a slow and fast region, of drug release. Initially, FEN release is extremely slow until a certain time denoted as the lag time, determined by the intersection of the linear extrapolation of the initial slow dissolution region (over which less than 5% of the drug dissolution occurs) and the subsequent fast dissolution region (see Figure S5 in the Supporting Information). The delay in dissolution is due to the presence of a PVA shell on the composite hydrogels that prevents the FEN nanocrystals contained in the core from being dissolved. As the ALG beads became larger, the lag time of drug release was observed to increase. This indicates that the lag time is greatly influenced by the thickness of the PVA shell on the composite hydrogels. However, in the second phase of drug dissolution, FEN was released very rapidly from all composite hydrogel formulations. Almost 80% of drug dissolution occurs within 30 to 100 min,

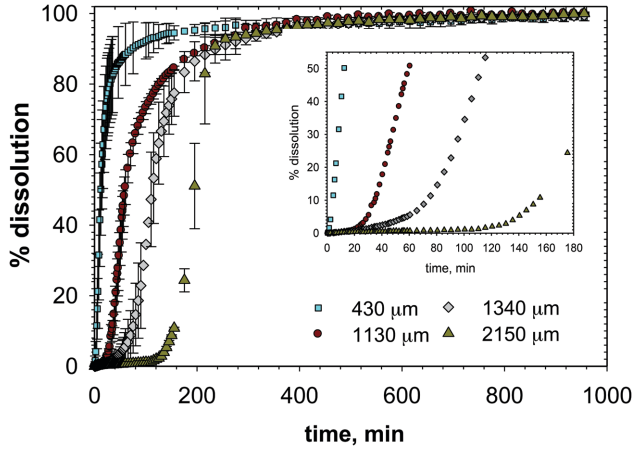

Figure 5. Dissolution profiles of FEN from dried composite core–shell hydrogels with different bead sizes prepared at ϕ = 30% (continuous phase: 2% w/v ALG aqueous solution with 1% w/v PVA; dispersed phase: anisole with $C_{FEN} = C_{satFEN}$). Dissolution was performed at 37 °C and 75 rpm. Each value represents the mean ± SD (n = 4).

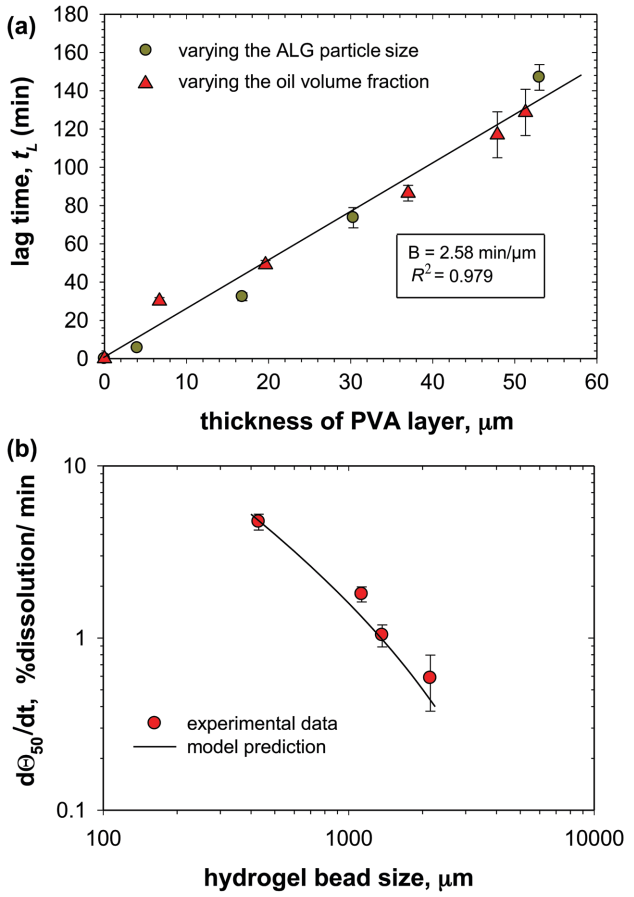

Figure 6. a) Lag time is plotted versus the thickness of the PVA layer on the composite hydrogel. Lag time measurements correspond to core–shell hydrogel particles produced either by varying the overall ALG particle size (at ϕ = 30%, circles) or varying the volume fraction at constant PVA concentration (1% w/v in the continuous phase, triangles). The correlation between lag time and shell thickness is determined by fitting the data with Equation (3) (line), shown in the box with the R^2 value. b) Rate of dissolution $d\Theta/dt$ (at 50% API dissolution, symbols) is plotted as a function of the size of the core–shell composite hydrogel beads relative to predictions from the dissolution model represented by Equation (4) (line).

depending on the ALG bead size. In particular, hydrogel beads that are smaller in size (≈ 430 μm) have no significant lag time and the release is very fast (80% drug dissolved within 30 min).

The characteristic features of the dissolution profiles presented in Figure 5 demonstrate that API release from our composite particles is a two-part process. With reference to the final form of the core–shell particles shown in Figure 1, the PVA shell must be removed before the core can be infiltrated with the suspending medium to initiate nanocrystal dissolution. Following solubilization of the API, it must diffuse a distance several orders of magnitude larger than the crystal itself to reach the surface of the porous hydrogel matrix before it is finally released. The timescale of this complete process can be understood by modeling the underlying mechanisms of mass transport.

To quantify the correlation between the lag time (from Figure 5) and the thickness of the PVA layer (measured from SEM), these values are plotted relative to each other in **Figure 6**a. The comparison of experimental results shows that lag time and shell thickness are linearly correlated with a proportionality constant of about 2.58 min μm^{-1}. The length of this lag time, t_L, can be predicted quantitatively by modeling the dissolution kinetics of the PVA layer of thickness, w. By developing a quantitative model, the necessary particle properties can be determined a priori for the synthesis of a vesicle with desirable dissolution characteristics.

The dissolution time of the PVA shell can be calculated once an analytical form of the diffusive PVA concentration profile in the surrounding fluid is derived. Assuming a pure, uniform solid shell, removal of PVA is driven by convective mass transport in the stirred vessel. The rate-limiting step of such a system is dissolution of the solid as indicated by a large Biot number, Bi_m, which is the ratio of the rates of convection and diffusion (see the Supporting Information). Mass transport in this system is represented by a purely diffusive boundary layer at the shell surface over which a pseudo steady-state diffusion profile is formed. The concentration at the particle surface is set by the solubility of PVA, C_s, and the concentration at the boundary layer interface is dictated by the conservation of mass flux from diffusion inside the boundary layer and convection outside. Additionally, the concentration dependence of PVA diffusivity must be accounted for to accurately represent the diffusive flux. Previous studies of diffusion in concentrated polyelectrolyte solutions suggest that mobility is dominated by a slow mode resulting from aggregate formation,[40,41] which is expected at concentrations near C_s such as at the PVA shell surface. Accordingly, we adopt a power law dependence of the form $D(C) = \alpha D_0 C^{-\gamma}$, where D_0 and C are the bare diffusion and concentration of PVA (in units of g L^{-1}), respectively.[41] Our experimental studies with PVA in the semidilute regime suggest a value of $\alpha = 0.005$ and the molecular weight dependence of the power law exponent for polyelectrolytes yields $\gamma = 0.0061 M_w^{0.35} = 0.298$.[41] Implementing the concentration dependence of diffusivity and the mixed boundary conditions described above while solving Fick's second law results in an analytical solution for the steady-state concentration profile (see the Supporting Information).

By balancing the mass flux into the boundary layer (using the PVA concentration profile) with the loss of mass from the shell surface, the total time to remove the shell can be estimated according to

$$t_L = \frac{\rho_s}{h\, C_\delta} w = Bw \tag{3}$$

where C_δ is the concentration of PVA at the boundary layer interface. The slope, B, is a function of C_δ as well as the density of amorphous PVA, ρ_s, and the convective mass transport coefficient, h, resulting from the vessel stirring conditions. The value of C_δ is determined as the eigenvalue of $(1-\gamma)(1+1/Bi_m)(C_\delta/C_s) = 1-(C_\delta/C_s)^{1-\gamma}$, which is the analytical solution of the PVA concentration profile at the boundary layer interface. For the range of particle sizes studied here, a value of $C_\delta = 0.52 C_s$ was determined for all corresponding values of Bi_m (with variations less than 0.1%). Using literature values of characteristic PVA parameters ($D_0 = 3\times10^{-11}$ m^2 s^{-1}, $\rho_s = 1.27$ g mL^{-1}, $C_s = 0.8$ g mL^{-1}),[42] the proportionality constant is calculated as B = 2.5 min μm^{-1}, which agrees well with

Adv. Healthcare Mater. 2016,
DOI: 10.1002/adhm.201600266

the fitted value in Figure 6a. Hence, shell dissolution is a diffusion-limited process and Equation (3) provides an accurate estimate of the necessary shell thickness for a desired lag time in API dissolution.

The dependence of the dissolution rate (region 2 of API release in Figure 5) on drug loading and particle size can also be estimated by a simple mass transport model. Under United States Pharmacopeia (USP) dissolution experimental conditions, diffusion within the bead is the rate-limiting step. Thus, the flux of drug into solution is proportional to the drug concentration at the bead surface and the dissolution rate can be estimated by modeling the concentration profile inside the bead. The maximum rate (in the experimentally measured units of percent of total dissolved solid per minute) can be estimated according to

$$\frac{\partial}{\partial t}\left(\frac{C}{C_{\text{total}}}\right) = (100\%)\frac{6hC_{\max}(\tilde{r}=1,\tau)}{\phi D_{\text{p}} C_{\text{sat}}} \tag{4}$$

where C_{total} is the final concentration of API in the bulk and $C_{\max}$ is the largest estimated FEN concentration at the bead surface. Estimates of $C_{\max}$ are calculated by treating FEN dissolution as a two-step process involving nanocrystal dissolution then diffusion to the bead surface. The time scales of these processes differ by orders of magnitude and are therefore decoupled. Given that the nanocrystals are well dispersed, the hydrogel core is treated as a homogeneous sphere with a transient radial concentration profile. The "initial" concentration of the sphere evolves over time according to the transient radial concentration profile at half the average distance between the nanocrystals, which are treated as spheres with a constant surface concentration set at C_{satFEN}. Analytical solutions exist for both of these forms of transient diffusion. The maximum surface concentration is the product of these two mass transport processes, which results in a power law dependence on Bi_m (i.e., bead diameter) according to $C_{\max} \propto Bi_m^{C(\phi)}$, where the prefactor and exponent are functions of volume fraction (see the Supporting Information). Dissolution rates estimated using these values of $C_{\max}$ are shown in Figure 6b compared to experimental results (at $\phi = 30\%$), which show excellent agreement. The accuracy of our dissolution model indicates that the bead size controls the rate (and thus time) of dissolution, which results from the controlled crystallization on the nanoscale. This model is sufficiently general to represent the release of nanocrystals of any API. By removing crystal dissolution as a mass transport barrier, our composite hydrogels offer a method of rapid drug release coupled with a well-controlled lag time, if desired.

To further investigate the influence of the shell on the release behavior of FEN nanocrystals embedded inside the core, dissolution measurements were carried out using composite hydrogels without a shell. The PVA shell was removed by washing the composite hydrogels with water and then drying again at 60 °C. The ALG beads without the PVA layer exhibit faster release profiles without any lag time (Figure S6 in the Supporting Information). This result confirms that the densely packed PVA shell provides a diffusion barrier for the guest molecules embedded inside the confined environment of ALG core. Further, it offers additional customization of the final release profile by completing a simple post-production washing step of the initial core–shell beads.

Our study demonstrates that the drug dissolution patterns from core–shell composite hydrogels can be modulated through incorporating a lag phase of pre-established duration in their release profile by altering the thickness of a PVA shell. Currently, there is significant interest in programming a lag period of controllable duration in drug delivery systems, primarily in connection with oral chronotherapy and colon targeting.[37] Properly modulated lag phases prior to drug release may be advantageous in a number of instances. One example is avoiding undesired drug–drug interactions in the gastrointestinal track, which will comply with chronotherapeutic needs and thus improve the overall patient experience. Such delivery systems are often pursued through polymeric barriers in the form of a shell that encloses an inner drug formulation. Usually, hydrophilic polymers such as cellulosic derivatives, PVA, or polyethylene oxide (PEO) have been employed to prepare the polymeric barriers. These barriers or coatings have recently been manufactured by hot processing techniques (e.g., hot-melt extrusion, injection molding),[43] and spray coating[44] as well as laborious surface modification, such as layer-by-layer approach,[45] microfluidic synthesis using double emulsions.[23] However, our approach to prepare core–shell microspheres does not require any such state-of-the-art techniques. Overall, our formulation methodology provides a facile way to tailor drug release kinetics by taking advantage of the tunable properties of core–shell microstructured hydrogels. Furthermore, because of their biofriendly nature, and the adjustable nanocrystal size and drug loading capacity, our proposed composite core–shell hydrogels could potentially be integrated into a final solid formulation form (e.g., capsules or tablets) for oral delivery. Since the current methodology (nozzle/needle based centrifugal synthesis system) used in this study is limited to fabricating hydrogel beads with diameters greater than 200 µm, the current formulations are not yet appropriate for parenteral administration (intravenous/ subcutaneous administration) because of their size.[46] We are currently exploring other techniques to fabricate smaller hydrogel beads and further engineer the microstructures of the beads for not only faster dissolution kinetics, but also for applications in other advanced release systems.

3. Conclusion

In summary, we report composite hydrogel microparticles with core–shell structures and their use for formulating nanocrystals of water-insoluble APIs. We demonstrate the higher drug loading embedded inside a hydrogel core matrix with improved dissolution kinetics utilizing the advantages of a core–shell microstructure. The incorporation of hydrophobic nanodomains carrying the APIs inside the hydrogel matrix represents a promising formulation approach for improving the solubility and bioavailabilty of water-insoluble APIs. Furthermore, we can independently control the shell and crystal sizes to engineer a core–shell microstructure to quantitatively tune the drug dissolution kinetics, providing a versatile drug delivery vehicles. Our novel approach of simultaneous

controlled crystallization and formulation could potentially circumvent several energy intensive top–down processes in traditional manufacturing. With the ability to produce and formulate nanometer sized crystals with controlled size, adjustable drug loading capacity and tunable release properties, our proposed core–shell hydrogels could potentially serve as a final drug formulation that is even amenable to continuous manufacturing.[17] More generally, the versatility and orthogonal accessibility of the composite core–shell hydrogels opens up a wide range of applications such as the design of multi-drug therapies, the preparation of designer foods, delayed/pulsatile drug delivery and cell encapsulation. The proposed approach is not limited to only pharmaceutical products, but can also be useful to production of a wide range of crystalline nanomaterials.

4. Experimental Section

Materials: Fenofibrate (CAS no. 49562-28-9, >99% pure), anisole (CAS no. 100-66-3, >99% pure), calcium chloride (CAS no. 10043-52-4, >93% pure), sodium dodecyl sulfate (CAS no. 151-21-3, >99% pure), and polyvinyl alcohol (Mowiol 8-88, $M_w \approx 67\,000$, CAS no. 9002-89-5) were purchased from Sigma-Aldrich and used as received. Sodium alginate (CAS no. 9005-38-3), a polysaccharide consisting of ≈61% mannuronic (M) and 39% guluronic (G) acid was also purchased from Sigma. 14, 15, 20, and 22 gauge needles were purchased from Nordson EFD. DI water was used throughout the experiments.

Nanoemulsion Preparation and Characterization: To prepare the nanoemulsions, a pre-emulsion was first generated by adding the dispersed phase (anisole containing a saturated concentration of FEN) into the continuous phase (2% w/v sodium alginate solution containing 1% w/v PVA) using a magnetic stirrer bar for 30 min at 700 rpm. The dispersed phase of anisole saturated with FEN was prepared by bringing excessive amounts of FEN in contact with anisole to establish solid–liquid equilibrium at room temperature. The mother batch was allowed to equilibrate for 24 h at room temperature at 200 rpm stirring speed.

The pre-emulsion was then ultrasonicated in 5 mL aliquots at 30% amplitude in an ultrasonicator with a 24 mm diameter horn (from Cole Parmer) at a frequency of 20 kHz. Nanoemulsion droplet sizes were measured via dynamic light scattering (DLS) using a Wyatt Technology DynaPro NanoStar Instrument. Samples were diluted to $\phi = 0.001$ in deionized water. Autocorrelation functions were measured at a scattering angle of 90° and a temperature of 25 °C. Three independent measurements were taken for each sample. Each DLS measurement was taken over a 50 s acquisition. Size and polydispersity were extracted from raw DLS data using second-order cumulant analysis.

Procedure for Core–Shell Hydrogels Preparation: To prepare the core–shell hydrogel particles, uncrosslinked nanoemulsion solution contained in a 5 mL syringe was dripped into a $CaCl_2$ solution using a microfluidic positive displacement pump (KD Scientific 110). For the core–shell particles obtained at various volume fractions of dispersed phase (ϕ), a 15 gauge stainless steel blunt-tip needle was used for dripping, unless specified otherwise. The dripping height was set to 10 cm and the dripping bath containing 6% w/v $CaCl_2$ was stirred with a magnetic stirrer at 100 rpm. The resulting hydrated hydrogel particles were then washed by exchanging the calcium chloride cross-linking solution five times with deionized water. They were then filtered using a Buchner funnel and rinsed once more with deionized water. The nanoemulsion laden crosslinked hydrogels were then allowed to be dried in an oven at 60 °C for 2–4 d, leading to the formation of hydrogel materials with core–shell microstructures. The sizes of resulting composite core–shell hydrogels ranged from 1200 to 2000 µm depending on the volume fraction of dispersed phase used in the experiments. At constant dispersed phase (ϕ = 30%), various sized core–shell hydrogel particles were also generated following the above experimental procedures, but using different needle sizes. For example, 1130, 1340, and 2150 µm sized hydrogel beads were prepared using 22G, 20G, and 14G needles, respectively. However, to produce the 430 µm sized particles, centrifugal synthesis approach was used (the preparation method is described in the Supporting Information).

Loading Measurements: The nanoemulsion laden hydrogels are synthesized with different nanoemulsion volume fractions ranging between 10% and 40%. For each measurement of a given volume fraction, two batches of nanoemulsion laden hydrogels are prepared with the same method of emulsification followed by cross-linking. One is a reference batch without API and the other is a test batch carrying dissolved API at the saturation concentration. The samples from both batches (≈200 mg of ALG beads) are placed in a vacuum oven, dried over 3 d at 60 °C and then weighted. Drug loading is defined as the difference in weight between the dried test batch carrying API and the dried reference batch formulated without the API divided by the weight of dried test batch carrying API. Loading measurements were done in five replicates, the average of which are reported with sample standard deviations. The experimentally measured drug loading capacity is also compared to the predicted value calculated according to Equation (1).

Analysis of Core–Shell Hydrogel Materials: The dried composite core–shell hydrogels were analyzed by powder X-ray diffraction (PXRD) in reflectance mode (Panalytical X'pert MPD Pro). The samples were ground then placed on a zero background disk. The PXRD was operated at 40 kV, 30 mA, and at a scanning rate of 2° min^{-1} over the range of $2\theta = 10°–40°$, using Cu Kα radiation wavelength of 1.54 Å. Samples were also analyzed by differential scanning calorimetry (DSC) using TA Instruments (Q2000 DSC). 10–15 mg of sample was crimped in a sealed T-zero aluminum pan and heated at 10 °C min^{-1} in the range of –20 °C to 250 °C using an empty sealed pan as a reference. Dry nitrogen was used as purge gas and the N_2 flow rate was 50 mL min^{-1}. Raman spectra of the composite hydrogel with FEN nanocrystals embedded within it were obtained with the aid of Raman spectroscopy coupled to a Leica optical light microscope. The Raman microscope (Kaiser Optical Systems, Inc.) was equipped with a 450 mW external cavity stabilized diode laser as the excitation source, operating at 785 nm. The size and morphology of the composite hydrogel particles and the embedded FEN crystals were characterized with high-resolution scanning electron microscope (Zeiss HRSEM) at 5 kV accelerating voltage and at various magnifications. All samples were prepared on conventional SEM stubs with carbon tape and were coated with about 10–15 nm of Au-Pd by sputter coating. The images were later analyzed with ImageJ manually to calculate the mean particle and crystal size.

Dissolution Experiments: The in vitro dissolution of FEN from the prepared core–shell hydrogels was carried out using the standard USPII (paddle) apparatus at 37 °C and 75 rpm. The dissolution medium was 600 mL of 0.2 M phosphate buffer at pH 6.8, containing 0.72% w/v SDS. The pH value was chosen so that the hydrogels would be encouraged to swell[17] and, with the uptake of water, consequently release their drug contents. Samples of dried composite hydrogel formulation (equivalent to about 12.5 mg of drug) was added to the dissolution media manually. Given the loading of FEN and the saturation solubility of FEN in the media, the mass of FEN added for a dissolution experiment was at least three times less than the mass of FEN required to saturate the media, thus maintaining sink conditions during dissolution experiments. The UV measurements were obtained using an automatic Varian UV–Vis Cary 50 apparatus and in situ probe set. All reported measurements were repeated at least three times under identical conditions and averaged values are reported here.

Supporting Information

Supporting Information is available from the Wiley Online Library or from the author.

Acknowledgements

A.Z.M.B. and P.D.G. contributed equally to this work. The authors thank the Novartis-MIT Center for Continuous Manufacturing for financial support and use of instrumentation.

Received: March 11, 2016
Revised: April 19, 2016
Published online:

[1] J. U. Junghanns, R. H. Müller, *Int. J. Nanomed.* **2008**, *3*, 295.
[2] L. Gao, D. Zhang, M. Chen, *J. Nanopart. Res.* **2008**, *10*, 845.
[3] R. Shegokar, R. H. Müller, *Int. J. Pharm.* **2010**, *399*, 129.
[4] G. G. Liversidge, K. C. Cundy, *Int. J. Pharm.* **1995**, *125*, 91.
[5] C. M. Keck, R. H. Müller, *Eur. J. Pharm. Biopharm.* **2006**, *62*, 3.
[6] H. Chen, C. Khemtong, X. Yang, X. Chang, J. Gao, *Drug Discovery Today* **2011**, *16*, 354.
[7] V. B. Junyaprasert, B. Morakul, *Asian J. Pharm. Sci.* **2015**, *10*, 13.
[8] B. Van Eerdenbrugh, G. Van den Mooter, P. Augustijns, *Int. J. Pharm.* **2008**, *364*, 64.
[9] G. J. Vergote, C. Vervaet, I. Van Driessche, S. Hoste, S. De Smedt, J. Demeester, R. A. Jain, S. Ruddy, J. P. Remon, *Int. J. Pharm.* **2001**, *219*, 81.
[10] F. Liu, J. Y. Park, Y. Zhang, C. Conwell, Y. Liu, S. R. Bathula, L. Huang, *J. Pharm. Sci.* **2010**, *99*, 3542.
[11] R. M. Ramanan, P. Chellamuthu, L. Tang, K. T. Nguyen, *Biotechnol. Prog.* **2006**, *22*, 118.
[12] H. Eral, V. López-Mejías, M. O'Mahony, B. Trout, A. Myerson, P. Doyle, *Cryst. Growth Des.* **2014**, *14*, 2073.
[13] B. Baghaei, S. H. Jafari, H. A. Khonakdar, U. Wagenknecht, G. Heinrich, *J. Appl. Polym. Sci.* **2014**, *131*, 40625.
[14] D. Jagadeesan, I. Nasimova, I. Gourevich, S. Starodubtsev, E. Kumacheva, *Macromol. Biosci.* **2011**, *11*, 889.
[15] D. J. McClements, *Annu. Rev. Food Sci. Technol.* **2010**, *1*, 241.
[16] H. Z. An, M. E. Helgeson, P. S. Doyle, *Adv. Mater.* **2012**, *24*, 3838.
[17] H. Eral, M. O'Mahony, R. Shaw, B. Trout, A. Myerson, P. Doyle, *Chem. Mater.* **2014**, *26*, 6213.
[18] M. Mabrouk, D. R. Chejara, J. A. Mulla, R. V. Badhe, Y. E. Choonara, P. Kumar, L. C. du Toit, V. Pillay, *Int. J. Pharm.* **2015**, *490*, 429.
[19] D. Missirlis, R. Kawamura, N. Tirelli, J. A. Hubbell, *Eur. J. Pharm. Sci.* **2006**, *29*, 120.
[20] S. Jana, A. Samanta, A. K. Nayak, K. K. Sen, S. Jana, *Int. J. Biol. Macromol.* **2015**, *74*, 85.
[21] C. Wu, W. Fan, M. Gelinsky, Y. Xiao, J. Chang, T. Friis, G. Cuniberti, *J. R. Soc. Interface* **2011**, *8*, 1804.
[22] M. Guo, X. Cao, E. W. Meijer, P. Y. Dankers, *Macromol. Biosci.* **2013**, *13*, 77.
[23] J. Wu, T. Kong, K. W. Yeung, H. C. Shum, K. M. Cheung, L. Wang, M. K. To, *Acta Biomater.* **2013**, *9*, 7410.
[24] P. Erni, G. Dardelle, M. Sillick, K. Wong, P. Beaussoubre, W. Fieber, *Angew. Chem. Int. Ed.* **2013**, *52*, 10334.
[25] F. O. M. S. Abreu, C. Bianchini, T. B. L. Kist, M. M. C. Forte, *Polym. Int.* **2009**, *58*, 1267.
[26] P. Mukhopadhyay, S. Chakraborty, S. Bhattacharya, R. Mishra, P. P. Kundu, *Int. J. Biol. Macromol.* **2015**, *72*, 640.
[27] M. Ma, A. Chiu, G. Sahay, J. C. Doloff, N. Dholakia, R. Thakrar, J. Cohen, A. Vegas, D. Chen, K. M. Bratlie, T. Dang, R. L. York, J. Hollister-Lock, G. C. Weir, D. G. Anderson, *Adv. Healthcare Mater.* **2013**, *2*, 667.
[28] A. M. Yousaf, D. W. Kim, Y. K. Oh, C. S. Yong, J. O. Kim, H. G. Choi, *Int. J. Nanomed.* **2015**, *10*, 1819.
[29] A. Gupta, H. B. Eral, T. A. Hatton, P. S. Doyle, *Soft Matter* **2016**, *12*, 1452.
[30] R. A. L. Leon, A. Z. M. Badruddoza, L. Zheng, E. W. Q. Yeap, A. I. Toldy, K. Y. Wong, T. A. Hatton, S. A. Khan, *Cryst. Growth Des.* **2015**, *15*, 212.
[31] R. A. L. Leon, W. Y. Wan, A. Z. M. Badruddoza, T. A. Hatton, S. A. Khan, *Cryst. Growth Des.* **2014**, *14*, 140.
[32] L. M. Dwyer, V. K. Michaelis, M. O'Mahony, R. G. Griffin, A. S. Myerson, *CrystEngComm* **2015**, *17*, 7922.
[33] M. Van Speybroeck, V. Barillaro, T. D. Thi, R. Mellaerts, J. Martens, J. Van Humbeeck, J. Vermant, P. Annaert, G. Van den Mooter, P. Augustijns, *J. Pharm. Sci.* **2009**, *98*, 2648.
[34] Z. Jia, P. Lin, Y. Xiang, X. Wang, J. Wang, X. Zhang, Q. Zhang, *Eur. J. Pharm. Biopharm.* **2011**, *79*, 126.
[35] M. Van Speybroeck, R. Mellaerts, R. Mols, T. D. Thi, J. A. Martens, J. Van Humbeeck, P. Annaert, G. Van den Mooter, P. Augustijns, *Eur. J. Pharm. Sci.* **2010**, *41*, 623.
[36] M. J. Garvey, T. F. Tadros, B. Vincent, *J. Colloid Interface Sci.* **1974**, *49*, 57.
[37] C. Berkland, E. Pollauf, D. W. Pack, K. Kim, *J. Controlled Release* **2004**, *96*, 101.
[38] M. A. Mazumder, N. A. Burke, F. Shen, M. A. Potter, H. D. Stöver, *Biomacromolecules* **2009**, *10*, 1365.
[39] Y. Gao, D. Zhao, M. Chang, Z. Ahmad, J. Li, *Chem. Eng. J.* **2016**, *284*, 963.
[40] J. J. Tanahatoe, M. E. Kuil, *J. Phys. Chem. B* **1997**, *101*, 9233.
[41] M. Sedlák, E. J. Amis, *J. Chem. Phys.* **1992**, *96*, 826.
[42] C. M. Hassan, N. A. Peppas, *Adv. Polym. Sci.* **2000**, *153*, 37.
[43] A. Maroni, L. Zema, M. Cerea, A. Foppoli, L. Palugan, A. Gazzaniga, *J. Drug Delivery Sci. Technol.* **2016**, *32*, 229.
[44] A. Maroni, L. Zema, G. Loreti, L. Palugan, A. Gazzaniga, *Int. J. Pharm.* **2013**, *457*, 362.
[45] S. Saha, S. C. J. Loo, *J. Mater. Chem. B* **2015**, *3*, 3406.
[46] S. Jaspart, G. Piel, L. Delattre, B. Evrard, *Expert Opin. Drug Delivery* **2005**, *2*, 75.